



# Numerical modeling of hydrocarbon generation in the Douglas Formation of the Athabasca basin (Canada) and implications for unconformity-related uranium mineralization



Guoxiang Chi <sup>\*</sup>, Zenghua Li, Kathryn Bethune

Department of Geology, University of Regina, 3737 Wascana Parkway, Regina, Saskatchewan S4S 0A2, Canada

## ARTICLE INFO

### Article history:

Received 5 September 2013

Accepted 24 October 2013

Available online 1 November 2013

### Keywords:

Athabasca basin  
Douglas Formation  
Hydrocarbon generation  
Unconformity-related  
Uranium deposits  
Fluid flow

## ABSTRACT

The Proterozoic Athabasca Basin in Canada is known for its world-class, high-grade uranium deposits developed near the unconformity between the basin and the basement. The Douglas Formation in the upper part of the preserved strata in the basin contains total organic carbon (TOC) of up to 3.56 wt.%. Previous studies of organic matter maturation and hydrocarbon inclusions indicate that oil and gas have been generated from this formation, and that some hydrocarbons found in the unconformity-related uranium deposits were derived from the Douglas Formation. This study aims to evaluate how the oil and gas generation processes may have affected the fluid overpressure development in the basin, and whether or not the hydrocarbons generated in the Douglas Formation could migrate downward to stratigraphically lower intervals and eventually to the sites of mineralization near the unconformities. We carried out a series of numerical experiments to examine fluid overpressures, flow directions, temperatures, and oil and gas generation processes using a two-dimensional conceptual model derived from a geologic cross-section from the basin center to the eastern margin. An additional 5 km strata were added to current basin stratigraphy to account for observed paleogeothermal data. Variation studies were undertaken to account for uncertainties in the lithologies of the eroded strata, and the wide ranges of possible permeabilities of different lithologies and kinetic parameters of oil and gas generation. It is found that, if moderate permeabilities are used in the modeling for each lithology (known as the base model), oil and gas generation processes contribute little to the development of fluid overpressure, and fluid pressure in the basin is close to hydrostatic regardless of whether or not hydrocarbon generation in the Douglas Formation is included in the modeling. However, if permeabilities are assigned values one order of magnitude lower than in the base model, significant fluid overpressures are developed in the eroded strata in the upper part of the model. In the base model, oil generated in the Douglas Formation may migrate downward, driven by an overpressure zone situated above the Douglas Formation, but gas migrates upward. In the low-permeability model, however, the overpressures developed above the Douglas Formation are so high that both oil and gas generated in the Douglas Formation migrate downward. The numerical modeling results thus indicate that it is hydrodynamically possible for oil and gas generated in the Douglas Formation to migrate to the base of the basin and reach the sites of the unconformity-related uranium deposits.

© 2013 Elsevier B.V. All rights reserved.

## 1. Introduction

The formation of the world-class, high-grade uranium deposits related to the Early Proterozoic Athabasca basin in northern Saskatchewan, Canada requires that large amounts of fluids flowed through the sites of mineralization. It is generally agreed that the mineralizing fluids were brines derived from the basin (e.g., Alexandre et al., 2005; Cuney et al., 2003; Derome et al., 2005; Kyser et al., 2000; Mercadier et al., 2012; Richard et al., 2011), but the driving forces for the basinal fluids to migrate to the unconformity between the basin and the basement, where uranium mineralization took place, are still not well understood

(Chi et al., 2011). Various fluid-flow models have been proposed or implied for the Athabasca basin in previous studies, including large-scale convection related to effects of the thermal gradient (Boiron et al., 2010; Hoeve and Sibbald, 1978; Raffensperger and Garven, 1995) and deposit-scale convection related to heat anomalies associated with the high heat conductivity of graphite (Hoeve and Quirt, 1984), gravity-driven flow (Alexandre and Kyser, 2012; Derome et al., 2005), compaction-driven flow (Hiatt and Kyser, 2007), and deformation-induced fluid flow (Cui et al., 2012). In order to evaluate these potential fluid flow models, and eventually use them to predict favorable sites of mineralization based on the reverse engineering approach (e.g., L. Zhang et al., 2011; Y. Zhang et al., 2011; Zhao et al., 2012a), it is important to know the background fluid pressure and temperature of the basin, as they provide constraints on initial and boundary

<sup>\*</sup> Corresponding author.

E-mail address: [guoxiang.chi@uregina.ca](mailto:guoxiang.chi@uregina.ca) (G. Chi).

conditions. A previous study has shown that fluid overpressure caused by sediment compaction was small in the Athabasca basin, and that the fluid pressure within the basin was near the hydrostatic regime throughout the sedimentation history (Chi et al., 2013). It was also shown that the thermal profile of the basin was not disturbed by the slow fluid flow related to sediment compaction (Chi et al., 2013).

Although the Athabasca basin is generally characterized by reddish lithologies, which are poor in organic matter, the upper part of the preserved basin stratigraphy, particularly the Douglas Formation, is known to contain significant amounts of organic matter, with total organic carbon (TOC) up to 3.56 wt.% (Stasiuk et al., 2001). An average vitrinite reflectance equivalent value of 1.4% Ro in the Douglas Formation suggests a maximum burial temperature of 160° to 200 °C, which corresponds to the late oil to early dry gas zone of thermal maturity (Stasiuk et al., 2001). Furthermore, oil inclusions have been identified in the shales and siltstones of the Douglas Formation as well as in sandstones in the underlying formations (Stasiuk et al., 2001). It is widely accepted that the generation of oil and gas, with accompanying volume increase due to transformation of organic matter from solid to liquid or gas, is one of the most important mechanisms causing fluid overpressure, next to sediment compaction (Swarbrick et al., 2002), as demonstrated for example by numerical modeling for the Paleozoic Anticosti basin in eastern Canada (Chi et al., 2010) and the Paleozoic–Mesozoic Ordos basin in northern China (Xue et al., 2011). In the case of the Athabasca basin, however, it remains to be determined how the generation of hydrocarbons in the Douglas Formation may have affected the fluid pressure regime and fluid flow pattern in the basin.

Hydrocarbons have been documented in many of the uranium deposits in the Athabasca basin, and their origins and roles in uranium mineralization have been debated for a long time (e.g., Annesley et al., 2001; Hoeve and Sibbald, 1978; Kyser et al., 1989; Landis et al., 1993; Leventhal et al., 1987; McCready et al., 1999; Stasiuk et al., 2001; Wilson et al., 2007). In the original unconformity-type uranium mineralization model, Hoeve and Sibbald (1978) suggested that mineralization took place when a uranium-bearing, oxidizing fluid from the basin mixed with a reduced fluid from the basement near the unconformity, with the reductant (methane) being derived from nearby graphite-rich zones in the basement. Leventhal et al. (1987) and Kyser et al. (1989) argued that the bitumen found in the ores was not derived from graphite based on the carbon isotope compositions of the bitumen and graphite, and Leventhal et al. (1987) suggested that the hydrocarbons were emplaced after uranium mineralization. Wilson et al. (2007) provided biomarker evidence to indicate that at least part of the bitumen in the ores was sourced from the Douglas Formation, and also suggested that the bitumen postdates the ores and did not play any role in mineralization. Putting aside the controversy about the relative timing of bitumen and mineralization, it is of interest for this paper to examine whether or not the hydrocarbons generated in the Douglas Formation could have migrated to the basal part of the basin and the top of the basement.

Numerical modeling has been widely used to simulate fluid flow and chemical reaction processes in various geological environments including mineralization systems (e.g., Appold and Garven, 2000; Bethke and Marshak, 1990; Cathles, 1981; Chi and Savard, 1998; Chi and Xue, 2011; Chi et al., 2006, 2011, 2013; Garven, 1985, 1995; Gow et al., 2002; Hobbs et al., 2000; Ingebritsen, and Appold, 2012; Ju et al., 2011; Lin et al., 2003, 2006, 2008, 2009; Liu et al., 2005, 2008; Norton, 1978; Oliver et al., 2006; Ord et al., 2002; Schaub and Zhao, 2002; Schmidt Mumm et al., 2010; Sorjonen-Ward et al., 2002; Xing et al., 2008; Xue et al., 2010, 2011; Zhang et al., 2003, 2008; L. Zhang et al., 2011; Y. Zhang et al., 2011; Zhao et al., 2008a) and geoenvironmental systems (e.g., Awadh et al., 2013; Charifo et al., 2013; Khalil et al., 2013; Mugler et al., 2012; Sung et al., 2012; Zhao et al., 2010, 2011, 2012b). The simulated numerical models have varied from generic models (e.g., Zhao et al., 1997, 2004, 2007) to realistic geological conceptual models (e.g., Liu et al., 2010, 2011; Zhao et al., 2008b). In terms of simulating chemical reaction processes, the simulated system

can involve either single chemical reaction (e.g., Zhao et al., 2008c, 2008d,) or multiple complicated chemical reactions that take place in real rocks (e.g., Alt-Epping and Zhao, 2010). Numerical modeling was also used to simulate fluid flow, heat transfer and hydrocarbon transport in sedimentary basins (e.g., Chi et al., 2010; Garven, 1989; Zhao et al., 1999). As a result of this wide range of applications, numerical modeling has now become an indispensable method for dealing with a broad range of geoscience and geoenvironmental problems (Zhao et al., 2009).

In this paper, numerical modeling was carried out to examine the effect of hydrocarbon generation in the Douglas Formation on fluid pressure and fluid flow patterns in the Athabasca basin, built on a previous numerical modeling of fluid pressure related to sediment compaction in the same basin (Chi et al., 2013). The potential for hydrocarbons to migrate from the Douglas Formation to stratigraphically lower successions and the basement is evaluated, and the implications for uranium mineralization are also discussed.

## 2. Geological setting

The Athabasca basin is a Paleoproterozoic to Mesoproterozoic basin of mainly siliciclastic rocks resting unconformably on Archean to Paleoproterozoic basement (Card et al., 2007; Jefferson et al., 2007; Ramaekers et al., 2007). The western part of the basin is underlain by basement rocks belonging to the Taltson magmatic zone and the Rae Province, and the eastern part by the Hearne Province, which is bounded in the east by the Trans-Hudson orogen (Fig. 1a). Both the Rae and Hearne provinces are divided into different domains, of which the Mudjatik and Wollaston domains underlie the eastern part of the Athabasca basin, where the most important uranium deposits are situated (Fig. 1a). The basement rocks consist of Archean granitoid gneiss and metasedimentary rocks (mainly in Rae) and metavolcanic rocks (mainly in Hearne), overlain by Paleoproterozoic metasedimentary rocks, which are divided into the Murmac Bay, Thluicho Lake and Martin groups in Rae, and the Hurwitz Group and partly coeval Wollaston Supergroup in Hearne (Card et al., 2007).

The flat-lying, unmetamorphosed sedimentary rocks in the Athabasca basin belong to the Athabasca Group, which is divided into the following formations (from oldest to youngest): Fair Point, Read, Smart (may be a distal facies equivalent to Read), Manitou Falls, Lazenby Lake, Wolverine Point, Locker Lake, Otherside, Douglas, and Carswell (Fig. 1b; Ramaekers et al., 2007). Most of these formations are composed of sandstone with less than 5% of shale, except for the Wolverine Point Formation which comprises quartz arenite with abundant mudstone in the lower part, the Douglas Formation consisting mainly of mudstone and siltstone, and the Carswell Formation comprising mainly carbonates. The Douglas Formation is characterized by thin-laminated, black, carbonaceous mudstone and siltstone, with TOC ranging from < 0.25 to 3.56 wt.% (Stasiuk et al., 2001), and an average TOC of 0.74 wt.%. Detailed subdivisions of the formations and their lithologies are described by Ramaekers et al. (2007) and summarized in Chi et al. (2013).

It has been estimated that more than 5 km of strata may have been eroded above the youngest preserved rocks in the basin, based on fluid inclusion data from the Carswell structure and the Rumpel Lake drill core in the central part of the basin, which suggest a paleogeothermal gradient of 35 °C/km (Pagel, 1975). A similar estimate is also derived from the maximum burial temperatures of 160° to 200 °C for the Douglas Formation based on organic matter maturation (Stasiuk et al., 2001), assuming a thermal gradient of 35 °C/km. However, the lithologies of the eroded strata are unknown. The age and duration of sedimentation in the basin has been loosely constrained to be from 1760 Ma to 1500 Ma (Ramaekers et al., 2007), based on estimation of a ca. 1750 Ma age for onset of rapid erosion of the Trans-Hudson orogen (Alexandre et al., 2009; Annesley et al., 1997; Kyser et al., 2000; Orrell et al., 1999), a U–Pb age of 1644 ± 13 Ma for igneous zircon in a tuffaceous unit in the Wolverine Point Formation (Rainbird et al., 2007),

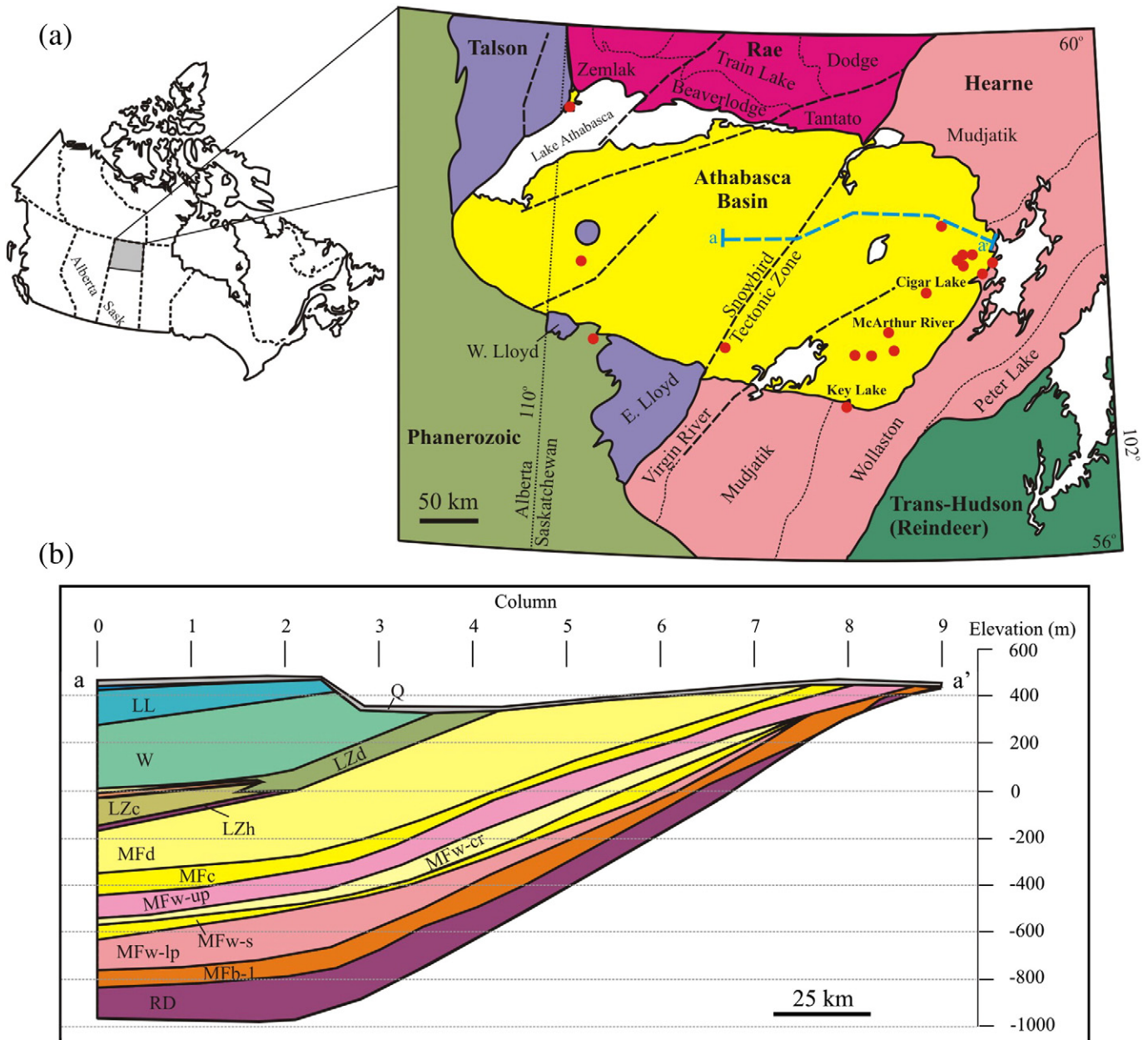


**Fig. 1.** a) Regional geologic framework of the Athabasca basin (modified from Card et al., 2007); red dots indicate the more important unconformity-related uranium deposits; b) a cross-section from the central part of the basin to the eastern margin (line a – a' in Fig. 1a) of the Athabasca basin (modified from Ramaekers et al., 2007), which is used as the basis of the physical model for the numerical modeling; RD – Read; MF – Manitou Falls (b – Bird; r – Raibl; w – Warnes; c – Collins; d – Dunlop); LZ – Lazenby Lake; W – Wolverine Point; LL – Locker Lake; O – Otherside; D – Douglas; Q – Quaternary.

and a Re–Os isochron age of  $1541 \pm 13$  Ma for carbonaceous shales in the Douglas Formation (Creaser and Stasiuk, 2007). A major primary uranium mineralization event is inferred to have occurred at  $\sim 1590$  Ma, based on LA-ICP-MS U–Pb dating of uraninite and Ar–Ar dating of syn-mineralization illite (Alexandre et al., 2009). This age suggests that the mineralization took place during sedimentation in the basin, before the deposition of the Douglas Formation. However, a spectrum of ages of uraninite younger than 1590 Ma has been reported, suggesting multiple uranium mineralization and/or uranium remobilization events during and after sedimentation (Jefferson et al., 2007; Kyser and Cuney, 2008).

### 3. Study methods and inputs

In order to evaluate how the generation of hydrocarbons in the Douglas Formation may have affected fluid pressure and fluid flow

patterns in the Athabasca basin, we carried out a series of two-dimensional numerical modeling to simulate the distribution and evolution of fluid pressure throughout the deposition history, and compared the results of models with hydrocarbon generation and those without hydrocarbon generation. We then calculated the impelling forces for oil and gas to examine the potential directions of hydrocarbon migration.

In a previous study by Chi et al. (2013), the effect of sediment compaction on fluid overpressure development, the most important among all potential overpressure-generating processes (Swarbrick et al., 2002), was simulated for the Athabasca basin using the program Basin2<sup>TM</sup> (Bethke et al., 1993). However, Basin2 does not have a module for hydrocarbon generation. Therefore, in the present study we used the program BsnMod, which was initially developed by Chi and Savard (1998) and Chi (2001), based on the mathematical model of Bethke (1985),

with a module for hydrocarbon generation being added by Chi et al. (2010). Both BsnMod and Basin2 use the finite difference method to solve related partial differential equations in a Lagrangian reference frame, which remains fixed with respect to the subsiding medium but moves through space. The finite difference grids are described in terms of a curvilinear coordinate, in which the  $x$  axis is parallel to the stratification and the  $z$  axis is vertical. Because the breadth of a sedimentary basin is generally much greater than its depth, the two axes can be considered approximately orthogonal (Bethke, 1985). This coordinate system can easily model the lateral change of strata thickness, without the need to use the finite element method which is commonly used to handle complex geometry. In addition, it has the advantage of keeping the  $x$  axis coincident with the maximum permeability, which is usually along stratigraphy in unfractured sedimentary rocks (Bethke, 1985). The governing equations (medium continuity, mass conservation, heat conservation, and hydrocarbon generation) and the numerical procedures are described in detail in Bethke (1985) and Chi et al. (2010), and the salient points are summarized in the Appendix. The use of the program BsnMod is described in Chi (2001), Chi et al. (2010) and Xue et al. (2011).

The geological conceptual model, which needs to be constructed in the first step of numerical modeling (Zhao et al., 2008b), is similar to the one used in Chi et al. (2013), which is based on a west–east cross-section compiled by Ramaekers et al. (2007). In this study, however, only the eastern half of the cross-section was modeled (Fig. 1b), with the left side being treated as a no-flow boundary. This treatment is based on the assumption that the basin is approximately symmetrical, and the central line represents a hydrogeologic divide. The strata in the model are divided into the following hydrostratigraphic units: 1) Read (R); 2) MFb-I (MF for Manitou Falls); 3) MFw-1p; 4) MFw-s; 5) MFw-cr; 6) MFw-up; 7) MFC; 8) MFd; 9) Hiatus 2; 10) LZh (LZ for Lazenby Lake); 11) LZc; 12) LZs; 13) LZl; 14) Wolverine Point (WP); 15) Hiatus 3; 16) Locker Lake (LL); 17) Otherside (O); 18) Douglas (D); 19) Carswell (C); and 20) Eroded strata (E). The modeled cross-section is divided into 10 evenly spaced columns, and the thicknesses of the different units at different columns were measured from Fig. 1b, and extrapolated where they are eroded at the top, except for the Otherside, Douglas and Carswell formations, for which maximum thicknesses of 183, 300 and 500 m (Ramaekers et al., 2007), respectively, were applied across the cross-section. The thickness of the eroded strata at the top of the model is assumed to be 5000 m, and the hiatuses

correlating with documented unconformities within the stratigraphy are represented by a thin layer (i.e., 1 m) of sediment. The start of sedimentation of the Read Formation is set at 1727 Ma, and the end of sedimentation of the Carswell Formation at 1469 Ma, following the time constraints shown in Fig. 7 of Jefferson et al. (2007). Assuming comparable sedimentation rates, a period of 50 Ma is assigned for the deposition of the assumed 5 km of eroded strata, such that sedimentation was finished by 1419 Ma. The durations of deposition of individual hydrostratigraphic units are interpolated from these ages as well as the two ages obtained for the Wolverine Point Formation (1644 Ma) and the Douglas Formation (1541 Ma), as discussed above. Each of the hiatuses is assigned a duration of 2 million years. These inputs (Table 1) are the same as those in Chi et al. (2013), except that the Fair Point Formation was not included in this study because it is not present in the eastern part of the basin. In addition, a TOC value of 0.1 wt.% was assigned to all units except for the Douglas Formation, which was given a TOC value of 0.74 wt.% in accordance with the average value calculated from the data of Stasiuk et al. (2001) (Table 1). The input thicknesses were multiplied by a decompaction factor in the calculation, such that the calculated total thicknesses after compaction are equal to those shown in Table 1. An average decompaction factor of 1.75 was estimated based on several try-and-error runs. The lithologies of individual units are represented by different proportions of sandstone, shale and carbonate (Table 1), which are based on the stratigraphic information presented in Ramaekers et al. (2007).

The rock, fluid, and hydrocarbon properties used in modeling, as well as the kinetic parameters of hydrocarbon generation and the parameters in the porosity–depth and porosity–permeability relation equations, all required as inputs in the BsnMod program, were adapted from Chi et al. (2010) and are summarized in Table 2. The boundary conditions are the same as those in Chi et al. (2013), except that the left boundary is closed to fluid flow as it is considered as a symmetry plane. The right and upper boundaries are open to fluid flow, and the bottom boundary impermeable. The surface temperature is fixed at 20 °C, and a heat flux of 71.8 mW/m<sup>2</sup> is supplied from the base of the model, which corresponds to the estimated thermal gradient of 35 °C/km. Variation studies were carried out by using different porosity–permeability parameters, the sand–shale proportions of the top eroded strata, the TOC contents, and the hydrocarbon kinetic parameters, as compared to those in Tables 1 and 2.

**Table 1**  
Lithology, time interval, thickness, and TOC of hydrostratigraphic units of the Athabasca basin as used in the numerical model.

Unit	Lithology*	End time (Ma)	Thickness (m)										TOC (wt.%)
			0	1	2	3	4	5	6	7	8	9	
Distance from the left boundary (km)			0	24.1	48.2	72.3	96.4	120.5	144.6	168.7	192.8	216.9	
Eroded strata	50% ss + 50% sh	1419	5000	5000	5000	5000	5000	5000	5000	5000	5000	5000	0.10
Carswell	90% cn + 5% ss + 5% sh	1469	500	500	500	500	500	500	500	500	500	500	0.10
Douglas	30% ss + 70% sh	1541	300	300	300	300	300	300	300	300	300	300	0.74
Otherside	95% ss + 5% sh	1582	183	183	183	183	183	183	183	183	183	183	0.10
Locker Lake	95% ss + 5% sh	1602	153	118	93	91	91	87	86	83	78	70	0.10
Hiatus 3	100% ss	1642	1	1	1	1	1	1	1	1	1	1	0.10
Wolverine Point	40% ss + 60% sh	1644	268	282	296	273	250	240	230	220	200	170	0.10
Lazenby Lake LZ1	98% ss + 2% sh	1652	15	14	12	11	10	10	10	10	10	10	0.10
LZs	98% ss + 2% sh	1654	24	22	20	18	15	15	15	15	15	15	0.10
LZc	98% ss + 2% sh	1656	112	78	44	45	45	48	50	48	43	40	0.10
LZh	98% ss + 2% sh	1666	20	20	20	15	10	10	10	10	10	10	0.10
Hiatus 2	100% ss	1667	1	1	1	1	1	1	1	1	1	1	0.10
Manitou Falls MFd	97% ss + 3% sh	1669	180	224	268	275	282	271	260	250	230	200	0.10
MFC	99% ss + 1% sh	1689	95	79	63	50	37	40	42	43	47	50	0.10
MFw-up	97% ss + 3% sh	1694	92	92	92	88	84	72	59	64	67	60	0.10
MFw-cr	97% ss + 3% sh	1701	29	36	43	65	86	66	45	20	0	0	0.10
MFw-s	99% ss + 1% sh	1704	65	45	25	25	24	31	38	18	0	0	0.10
MFw-lp	99% ss + 1% sh	1706	126	155	184	125	66	53	40	20	0	0	0.10
MFb-I	99% ss + 1% sh	1720	71	79	87	90	93	63	32	52	46	20	0.10
Smart/read	95% ss + 5% sh	1727	126	153	179	138	96	84	73	35	0	0	0.10

\* ss = Sandstone, sh = shale, cn = carbonate.

**Table 2**  
Parameters related to fluid and rock properties used in the modeling.

Parameter	Value	Unit	Reference
<i>Water properties</i>			
Thermal expansion coefficient	$\alpha = 5.0E-4$	(/oC)	(1)
Compressibility coefficient	$\beta = 4.3E-10$	(m.s2/kg or/Pa)	(1)
Heat capacity	$Cf = 4.2E+3$	(J/kg/oC)	(1)
Heat conductivity	$Kf = 0.63$	(W/m/oC)	(2)
<i>Rock properties</i>			
Density	$\rho r = 2.7E+3$	(kg/m3)	(1)
Heat capacity	$Cr = 0.84E+3$	(J/kg/oC)	(1)
Heat conductivity	$Kr = 2.5$	(W/m/oC)	(2)
<i>Hydrocarbon properties</i>			
Kerogen density	$\rho k = 1.45E+3$	(kg/m3)	(3)
Oil initial density	$\rho o = 9.0E+2$	(kg/m3)	(4)
Oil thermal expansion coefficient	$\alpha = 7.0E-4$	(/oC)	(5)
<i>Kerogen (type-II)-to-oil conversion</i>			
Pre-exponential factor for oil	$Ao = 2.92E+17$	(/h)	(6)
Activation energy for oil	$Eo = 215.2$	(kJ/mol)	(6)
<i>Oil-to-gas conversion</i>			
Pre-exponential factor for gas	$Ag = 3.6E+16$	(/h)	(7)
Activation energy for gas	$Eg = 230$	(kJ/mol)	(7)
<i>Porosities and permeabilities</i>			
<i>Sandstone</i>			
Initial porosity	$\phi 0 = 0.40$	No unit	(8)
Irreducible porosity	$\phi 1 = 0.10$	No unit	(8)
Porosity-depth parameter	$b = 0.50$	/km	(8)
Permeability-porosity constant A	$A = 15$	No unit <sup>a</sup>	(8)
Permeability-porosity constant B	$B = -3$	No unit <sup>a</sup>	(8)
Horizontal to vertical permeability ratio	$k_x/k_z = 2.5$	No unit	(8)
<i>Shale</i>			
Initial porosity	$\phi 0 = 0.55$	No unit	(8)
Irreducible porosity	$\phi 1 = 0.05$	No unit	(8)
Porosity-depth parameter	$b = 0.85$	/km	(8)
Permeability-porosity constant A	$A = 8$	No unit <sup>a</sup>	(8)
Permeability-porosity constant B	$B = -8$	No unit <sup>a</sup>	(8)
Horizontal to vertical permeability ratio	$k_x/k_z = 10$	No unit	(8)
<i>Limestone</i>			
Initial porosity	$\phi 0 = 0.40$	No unit	(9)
Irreducible porosity	$\phi 1 = 0.05$	No unit	(9)
Porosity-depth parameter	$b = 0.55$	/km	(9)
Permeability-porosity constant A	$A = 6$	No unit <sup>a</sup>	(9)
Permeability-porosity constant B	$B = -4$	No unit <sup>a</sup>	(9)
Horizontal to vertical permeability ratio	$k_x/k_z = 2.5$	no unit	(9)

References: 1) Bethke (1985); 2) Garven (1985); 3) Lee and Williams (2000); 4) Speight (2006); 5) Jones (2010); 6) Pepper and Corvi (1995); 7) Pepper and Dodd (1995); 8) Harrison and Summa (1991); 9) Kaufman (1994);

<sup>a</sup> The permeabilities calculated from these A and B values are in darcies.

#### 4. Results of numerical modeling

The numerical modeling results for fluid overpressure, fluid flow vectors, and oil and gas generation zones at the end of sedimentation (1419 Ma), using the inputs from Tables 1 and 2, are shown Fig. 2. A core zone of fluid overpressure is developed within the assumed eroded strata (Fig. 2a), as was also observed in the study considering the effect of sediment compaction alone (Chi et al., 2013). The maximum fluid overpressure is 68 bars at a depth of 4067 m, where the calculated fluid pressure is 438 bars, which is close to the hydrostatic value of 399 bars (assuming a water density of 1 g/cm<sup>3</sup>), and far from the lithostatic value of 996 bars (assuming a rock density of 2.5 g/cm<sup>3</sup>). The overall fluid flow pattern is characterized by upward and rightward (toward basin margin) flow, but downward flow is indicated in the strata immediately below the overpressure core, especially in the Carswell and Douglas formations (Fig. 2b). Both the active oil and gas generation zones are located within the top eroded strata by 1419 Ma (Fig. 2c); the oil and gas generation within the Douglas Formation was mostly completed (90%) from 1457 to 1450 Ma, and from 1445 to

1437 Ma, respectively (Fig. 3a). An experiment with TOC value of 0.1 wt.% assigned to all lithostratigraphic units (including the Douglas Formation) produced similar results, with the maximum fluid overpressure being 64 bars at a depth of 4067 m. The calculated fluid overpressure values in the Douglas Formation at the basin center are only slightly different (less than 1 bar) between the run with 0.74 wt.% TOC for the Douglas Formation and the one with 0.1 wt.% TOC, although the higher TOC content helps to achieve the maximum overpressure faster (Fig. 3b).

The above results indicate that there is little effect of oil and gas generation on fluid overpressure development in the Athabasca basin in the model using the default inputs specified in Tables 1 and 2, which is hereinafter referred to as the base model for comparison. Fluid pressures are close to hydrostatic values regardless of whether hydrocarbon generation is considered or not. Whether or not and how much higher fluid overpressures may be achieved under other conditions are evaluated by variation studies, the results of which are described below.

Because there is no record of the eroded strata at the top of the basin, there is much uncertainty regarding its lithological make-up. In the base model, the lithologies of this unit are composed of 50% sand and 50% shale. If the proportion of shale is increased to 80%, the maximum fluid overpressure increases to 139 bars, which is considerably higher than the base model (68 bars), but still low compared to the 582 bar difference between the hydrostatic and lithostatic values at that depth (3803 m).

It is well known that the permeability of a lithology may vary by more than one order of magnitude, and that this can have a significant impact on fluid overpressure evaluation (e.g., Chi et al., 2010; Harrison and Summa, 1991). Variation studies were carried out with the permeabilities of sandstone, shale, and limestone set at one order of magnitude higher and lower than the base model, referred to as the high-permeability model and the low-permeability model, respectively. Thus, the permeability was varied from  $\log k_x = 8\phi - 9$  to  $\log k_x = 8\phi - 7$  for shale, from  $\log k_x = 15\phi - 4$  to  $\log k_x = 15\phi - 2$  for sandstone, and from  $\log k_x = 6\phi - 5$  to  $\log k_x = 6\phi - 3$  for limestone. The simulation results indicate that the overpressure values attained in the basin center in the high-permeability model (Fig. 4, curve a) are significantly lower than those obtained in the base model (Fig. 4, curve b), with the maximum overpressure being so small (less than 10 bars) that the fluid pressures are nearly equal to the hydrostatic values (Fig. 4, curve a). The low-permeability model (Fig. 4, curve c), on the other hand, produced fluid overpressures much higher than the base model (Fig. 4, curve b); a maximum overpressure of 328 bars was achieved at a depth of 5035 m (Fig. 4, curve c), which is half the difference between the lithostatic and hydrostatic values at that depth (740 bars).

The kinetic parameters of kerogen-to-oil and oil-to-gas conversion can vary over a wide range of values (Pepper and Dodd, 1995; Peters et al., 2006). Two sets of variation studies were carried out: one assuming fixed oil-to-gas conversion parameters (Table 2) coupled with varying kerogen-to-oil parameters, and the other assuming fixed kerogen-to-oil conversion parameters (Table 2) coupled with varying oil-to-gas conversion parameters. For the first one, a minimum value of  $3.11 \times 10^{16}$ /h for Ao and 209.2 kJ/mol for Eo, and a maximum value of  $5.48 \times 10^{17}$ /h for Ao and 230.1 kJ/mol for Eo (Peters et al., 2006) were tested. For the second set, a minimum value of  $3.6 \times 10^{15}$ /h for Ag and 225.9 kJ/mol for Eg, and a maximum value of  $1.08 \times 10^{18}$ /h for Ag and 238.6 kJ/mol for Eg (Pepper and Dodd, 1995), were used. Simulation results indicate that although the timing of oil and gas generation changed with different kinetic parameters (Fig. 5a and b), the effect on fluid overpressure development is very small. That is, the overpressure values in the Douglas Formation at the basin center do not show any discernible changes with different oil generation kinetic parameters (Fig. 5c), and very small changes (less than 1 bar) were produced with different gas generation kinetic parameters (Fig. 5d).

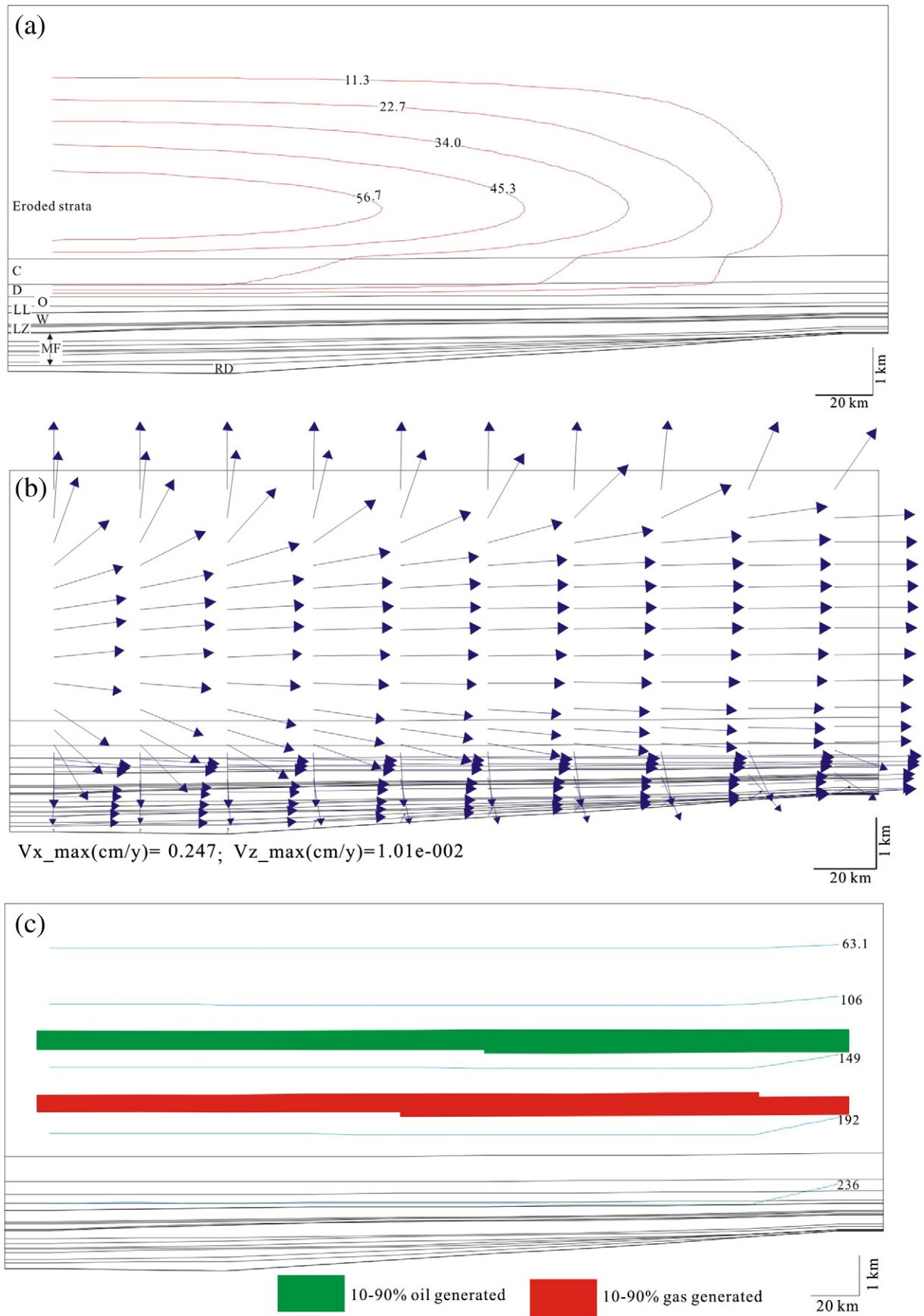
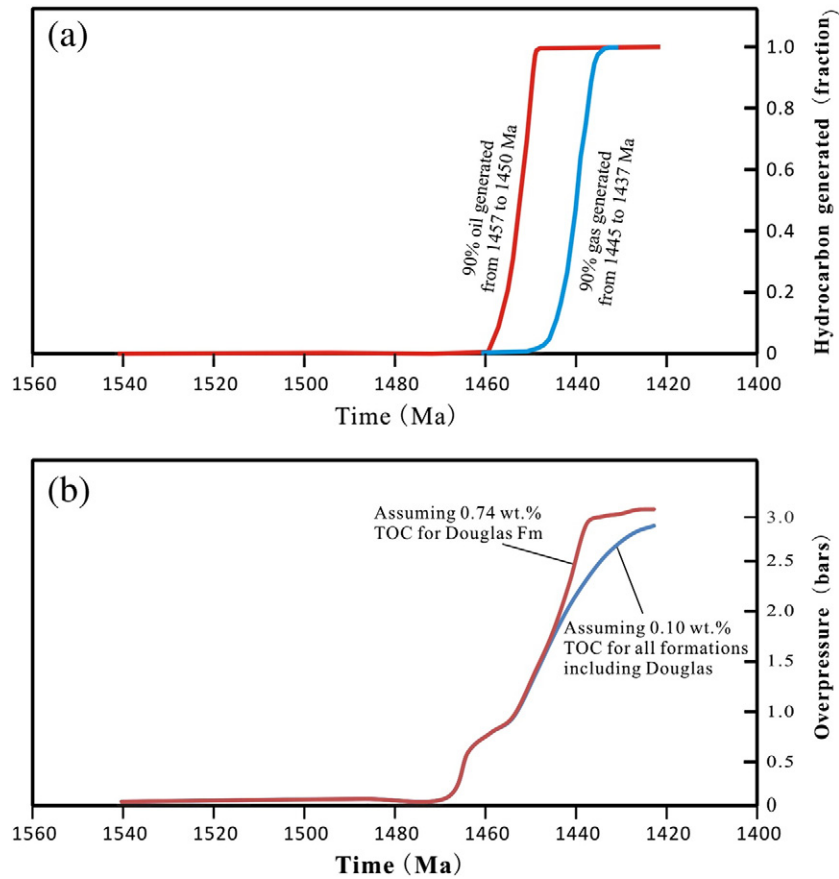


Fig. 2. Numerical modeling results of the base model (Table 1) showing a) contours of fluid overpressure (bars), b) fluid-flow direction (not to scale), and c) isotherms (°C) and oil and gas generation zones at the end of sedimentation at 1419 Ma.



**Fig. 3.** Numerical modeling results of the base model (Table 1) showing a) the time intervals of oil and gas generation in the Douglas Formation in the basin center, and b) the evolution of fluid overpressure in the Douglas Formation in the basin center, as compared to a model with 0.1 wt.% TOC.

Finally, a variation study with a TOC value of 3.56 wt.% (the maximum value reported in Stasiuk et al., 2001) being assigned to the Douglas Formation was tested. The results indicate that the maximum

fluid overpressure in the Douglas Formation in the basin center reached 4.8 bars, which is higher than that with a 0.74 wt.% TOC assumption (3 bars, Fig. 3b) but still not enough for the fluid pressure to deviate appreciably from the hydrostatic regime. Furthermore, the simulation results indicate that increasing the TOC value of the Douglas Formation to 3.56 wt.% does not have discernible effect on the maximum fluid pressure values attained within the eroded strata.

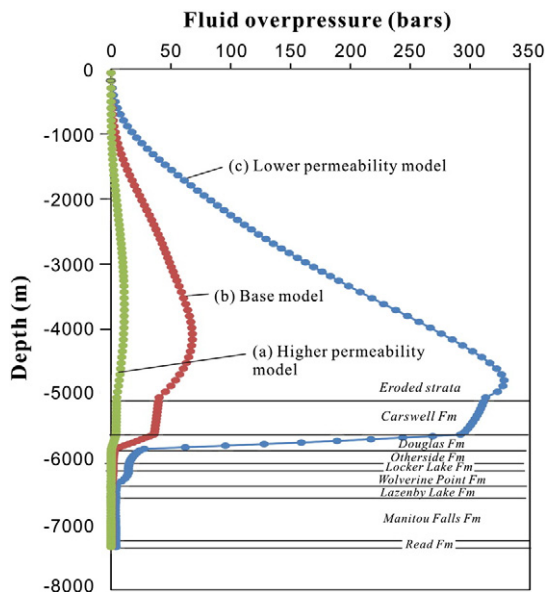


**Fig. 4.** Variation studies showing the profiles of fluid overpressures with depth at the basin center for three different permeabilities: a) permeabilities one order of magnitude higher than the base model (Table 2), b) the base model, and c) permeabilities one order of magnitude lower than the base model.

## 5. Discussion and conclusions

This paper has attempted to address two major questions regarding hydrocarbon generation in the Douglas Formation in the Athabasca basin, which are: 1) how much did the hydrocarbon generation processes affect the fluid overpressure development and fluid flow pattern in the basin? and 2) could the hydrocarbons generated in the Douglas Formation have migrated to the base of the basin and upmost basement, as recorded in some uranium deposits? The numerical modeling results presented above suggest that the hydrocarbon generation processes in the Douglas Formation contributed little to the development of fluid overpressure. In other words, fluid pressures in the basin remained close to the hydrostatic values regardless of whether or not oil and gas were generated in the Douglas Formation, unless very low permeabilities are assumed, especially for the assumed eroded strata at the top of the model (Fig. 4). This lack of influence of hydrocarbon generation on fluid overpressure development in the Athabasca basin, unlike some other basins such as the Anticosti and Ordos basins (Chi et al., 2010; Xue et al., 2011), may be related to the fact the majority of the strata underlying the Douglas Formation are highly permeable (> 95% sandstone), such that the overpressure caused by hydrocarbon generation in the Douglas Formation is easily dissipated.

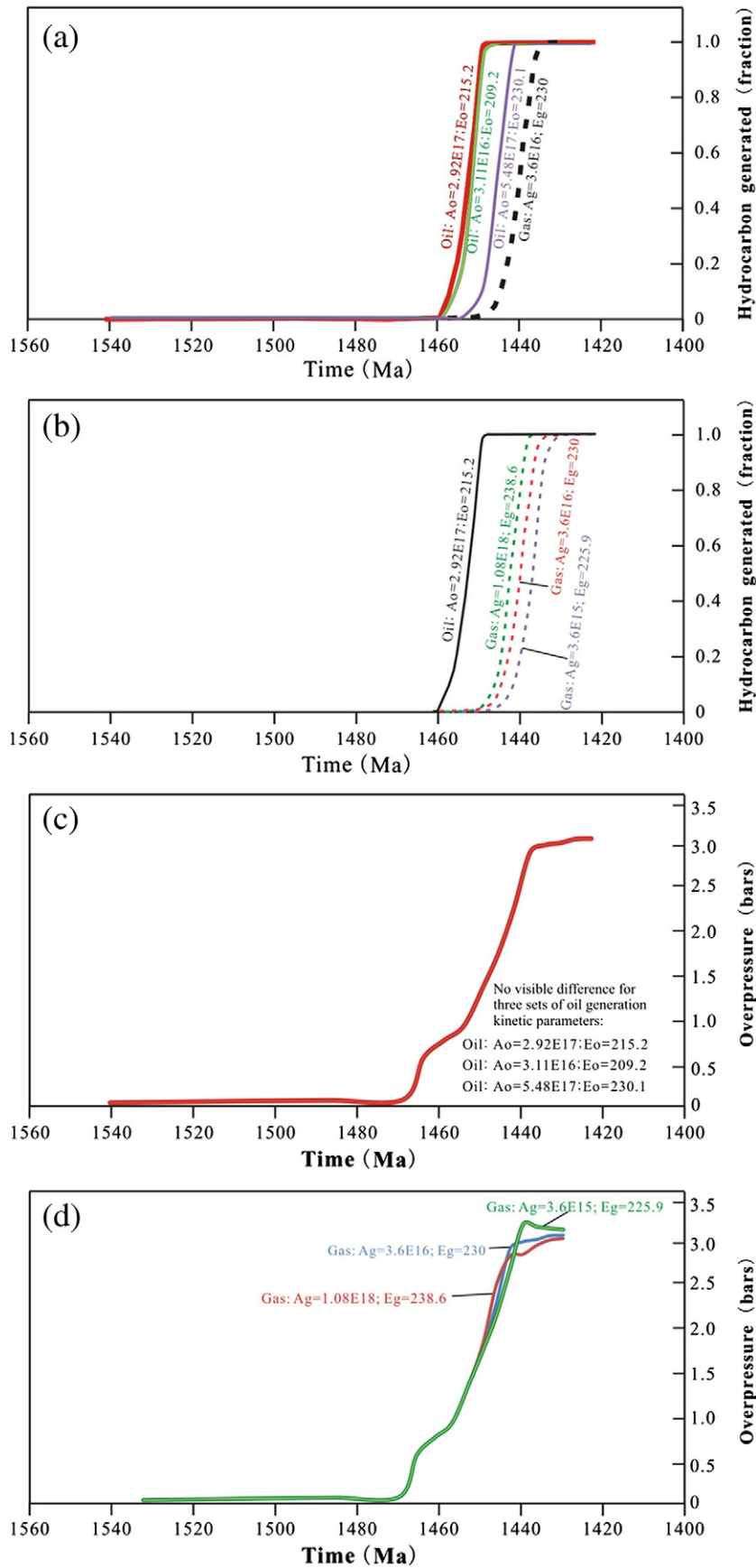


Fig. 5. Variation studies showing the different hydrocarbon generation curves with different kinetic parameters for oil (a) and gas (b), and the evolution curves of fluid overpressure in the Douglas Formation in the basin center for different kinetic parameters for oil (c) and gas (d).

The modeling results indicate that the Douglas Formation has experienced the oil and gas generation stages, which is consistent with the presence of oil inclusions and the Ro values confirming that the formation has been buried to the gas generation zone (Stasiuk et al., 2001). It remains to be evaluated whether or not and under what conditions the oil and gas generated in the Douglas Formation may have migrated to the base of the basin. The downward migration of hydrocarbons is decided by the vertical impelling force of hydrocarbons ( $E_{HC}$ ), which is related to fluid densities and fluid overpressure ( $\Psi$ ) as follows:

$$E_{HC} = \frac{\rho_W - \rho_{HC}}{\rho_{HC}} g + \frac{-1}{\rho_{HC}} \frac{\partial \Psi}{\partial z} \quad (1)$$

where  $\rho_{HC}$  is the density of oil or gas,  $\rho_W$  is the density of water, and  $g$  is gravity (Chi et al., 2010; Hubbert, 1953). The first term reflects the buoyancy force, which is positive (upward), and the second term is the impelling force caused by the fluid overpressure gradient, which is positive if fluid overpressure increases with depth or negative if fluid overpressure decreases with depth. The hydrocarbons will migrate upward if the  $E_{HC}$  value is positive, and downward if the  $E_{HC}$  value is negative.

Our numerical modeling results indicate that the maximum fluid overpressure is located within the assumed eroded strata at the top (Fig. 2a). Therefore, the fluid overpressure decreases with depth in the lower part of the basin, and fluid flow (water) is downward (Fig. 2b). In order to evaluate whether or not the hydrocarbons generated in the Douglas Formation can flow downward, we need to calculate the buoyancy forces for oil and gas and the impelling force caused by the fluid overpressure gradient. The calculated densities of water, oil, and gas in the Douglas Formation at the basin center are 0.90, 0.77 and 0.17 g/cm<sup>3</sup>, respectively. The buoyancy force for oil and gas is calculated to be 1.7 and 42.1 m s<sup>-2</sup>, respectively. In the base model, the maximum fluid overpressure is 67.5 bars at a depth of -4247 m, and the minimum overpressure is 0.41 bars at the base (-7341 m). The impelling force caused by the fluid overpressure gradient on oil and gas are calculated to be -2.8 and -12.8 m s<sup>-2</sup>, respectively. Combining the buoyancy force and the impelling force caused by fluid overpressure gradient, the vertical impelling force of hydrocarbons ( $E_{HC}$ ) is therefore -1.2 m s<sup>-2</sup> for oil and +29.3 m s<sup>-2</sup> for gas. In the variation study with low permeabilities (Fig. 4, curve c), where a maximum fluid overpressure of 328 bars was found at -5035 m, and a minimum of 4 bars at -7629 m, the impelling force caused by the fluid overpressure gradient on oil and gas are calculated to be -16.2 and -73.4 m s<sup>-2</sup>, respectively, resulting in an  $E_{HC}$  value of -14.5 m s<sup>-2</sup> for oil and -31.3 m s<sup>-2</sup> for gas.

The above calculations suggest that under the assumptions for the base model, the oil generated in the Douglas will theoretically migrate downward whereas the gas migrates upward. In the low-permeability model, however, both oil and gas generated in the Douglas Formation migrate downward, driven by the strong fluid overpressure developed within the assumed eroded strata above the Carswell Formation. It is worth noting here that minor evaporites have been found in the Carswell Formation (Ramaekers et al., 2007), and the possibility of massive evaporites being developed in the eroded strata at the top of the basin cannot be ruled out. In fact, the high salinities of fluid inclusions found in quartz overgrowths in the basin (e.g., Pagel, 1975; Scott et al., 2011) and in uranium deposits (e.g., Derome et al., 2005), especially the Cl/Br and  $\delta^{37}\text{Cl}$  analyses (Richard et al., 2011), suggest an evaporated seawater origin for the basinal brines in the Athabasca basin. Evaporites are known for their extremely low permeabilities, lower than shales (Kaufman, 1994), and if they were indeed developed in the upper part of the basin (now eroded), fluid overpressures may have been much higher than previously anticipated (Chi et al., 2013), and downward migration of hydrocarbons generated in the Douglas Formation would likely be most viable.

Finally, although it is not the main topic of discussion in this paper, it is worth mentioning that the timing of hydrocarbon emplacement in the uranium deposits remains an unsolved problem. The fact that solid bitumen crosscuts uraninite ores does not necessarily indicate that hydrocarbon migration postdates mineralization, as argued for by Leventhal et al. (1987) and Wilson et al. (2007). We suggest that even if hydrocarbons were involved in mineralization (i.e., emplaced before or during mineralization), they could remain as fluids after mineralization and flow into fractures in the ores to become solidified as bitumen. In addition, although the primary uranium mineralization age of 1590 Ma (Alexandre et al., 2009) is older than the estimated age of the Douglas Formation (1541 Ma, Creaser and Stasiuk, 2007), a number of younger ages of uraninite have also been reported (see Jefferson et al., 2007; Kyser and Cuney, 2008). Therefore, it is not impossible for hydrocarbons generated in the Douglas Formation to have migrated to the sites of mineralization and played a role in uranium mineralization.

In conclusion, our numerical modeling results indicate that oil and gas generation in the Douglas Formation has had minor effects on fluid overpressure development and fluid flow patterns in the Athabasca basin. If the 5 km of eroded sediment above the preserved strata are assumed to be composed of 50% shale and 50% sand, and the permeabilities are moderate (i.e., the base model), the fluid overpressures developed within this layer are so small that the fluid pressures are essentially hydrostatic. Despite this, the fluid overpressure gradient is sufficient to drive oil generated in the Douglas Formation downward, although gas migrates upward. In contrast, if the permeabilities are taken to be one order of magnitude lower than the base model, fluid overpressures generated in the eroded strata are significantly higher, and both oil and gas generated in the Douglas Formation are driven downward. This study therefore confirms that it is hydrodynamically possible that some hydrocarbons found in the unconformity-related uranium deposits were derived from the Douglas Formation, as suggested by biomarkers studies.

## Acknowledgments

This study is supported by an NSERC-Discovery grant (to Chi) and the TGI-4 (Targeted Geoscience Initiative 4) uranium ore systems program led by the Geological Survey of Canada, Natural Resources Canada (through a grant to Bethune and Chi).

## Appendix A. Governing equations and numerical solution procedure

The governing equations describing sediment compaction (medium continuity) (Eq. (2)), mass conservation (fluid continuity) (Eq. (3)) and heat conservation (Eq. (4)), from Bethke (1985), Harrison and Summa (1991), and Chi et al. (2010), are as follows:

$$\frac{\partial}{\partial z} v_{zm} = \frac{1}{(1-\phi)} \frac{\partial \phi}{\partial t} \quad (2)$$

$$\begin{aligned} \phi \beta \frac{\partial \psi}{\partial t} - \frac{1}{\rho} \left[ \frac{\partial}{\partial x} \left( \frac{\rho k_x}{\mu} \frac{\partial \psi}{\partial x} \right) + \frac{\partial}{\partial z} \left( \frac{\rho k_z}{\mu} \frac{\partial \psi}{\partial z} \right) \right] \\ = \phi \beta \rho v_{zm} \frac{1}{(1-\phi)} \frac{\partial \phi}{\partial t} + \phi \alpha \frac{\partial T}{\partial t} + q_o + q_g \end{aligned} \quad (3)$$

$$\begin{aligned} [\rho_f C_f + \rho_r (1-\phi) C_r] \frac{\partial T}{\partial t} - \frac{\partial}{\partial x} \left( K_x \frac{\partial T}{\partial x} \right) - \frac{\partial}{\partial z} \left( K_z \frac{\partial T}{\partial z} \right) + \\ \frac{\partial}{\partial x} (\rho v_x C_f T) + \frac{\partial}{\partial z} (\rho v_z C_f T) = -\rho h_f \frac{\partial \phi}{\partial t} \end{aligned} \quad (4)$$

where  $v_{zm}$  is the settling velocity of the solid medium,  $x$  is the horizontal coordinate,  $z$  is the vertical coordinate,  $t$  is time,  $\phi$  is porosity,  $\beta$  is the compressibility coefficient of fluid,  $\psi$  is fluid overpressure,  $\rho$  is the density of fluid,  $k_x$  is the horizontal permeability,  $k_z$  is the vertical permeability,  $\mu$  is the dynamic viscosity of fluid,  $\alpha$  is the thermal expansion

coefficient of fluid,  $T$  is temperature,  $q_o$  is the source term for oil generation,  $q_g$  is the source term for gas generation,  $C_f$  is the heat capacity of fluid,  $\rho_r$  is the density of rock,  $C_r$  is the heat capacity of rock,  $K_x$  is the horizontal heat conductivity,  $K_z$  is the vertical heat conductivity,  $v_x$  is the horizontal fluid flow velocity,  $v_z$  is the vertical fluid flow velocity, and  $h_f$  is the enthalpy of fluid. The values of  $q_o$  and  $q_g$  in Eq. (3) are related to density changes from kerogen to oil and from oil to gas as follows (Chi et al., 2010):

$$q_o = \frac{dX_o}{dt} \left( \frac{\rho_k}{\rho_o} - 1 \right) X_k V_b \quad (5)$$

$$q_g = \frac{dX_g}{dt} \left( \frac{\rho_o}{\rho_g} - 1 \right) X_k X_o V_b \quad (6)$$

where  $X_o$  and  $X_g$  are the fractions of oil and gas generated (out of the total capacity for oil and gas generation, respectively),  $t$  is time,  $\rho_k$ ,  $\rho_o$  and  $\rho_g$  are the density of kerogen, oil, and gas, respectively,  $X_k$  is the volume fraction of kerogen in sedimentary rocks, and  $V_b$  is the volume of a finite difference block.  $X_o$  and  $X_g$  are related to the generation rates of oil and gas as follows (Chi et al., 2010):

$$X_o = 1 - (1 - X_o^p) e^{-k_o \Delta t} \quad (7)$$

$$X_g = 1 - (1 - X_g^p) e^{-k_g \Delta t} \quad (8)$$

where  $\Delta t$  is time interval between two time steps,  $X_o^p$  and  $X_g^p$  are the fractions of oil and gas generated in the previous time step, and  $k_o$  and  $k_g$  are the generation rate of oil and gas, respectively.

The governing Eqs. (2)–(4) are first transformed into a curvilinear coordinate system, where the  $x$  axis is parallel to the stratification and the  $z$  axis is vertical, and then converted into algebraic equations using the finite difference method. The numerical procedure starts with an initial sedimentary layer set at hydrostatic conditions, and proceeds with the addition of a thin layer of sediment in each time step. For each time step, the sediment compaction equation (Eq. (2)) is first solved in conjunction with the following equations describing the relationship between effective depth and porosity (Bethke, 1985):

$$\phi = \phi_0 e^{z/b} + \phi_1 \quad (9)$$

$$z_e = z + \frac{\psi - \psi_{sc}}{\rho_{sm} - \rho} \quad (10)$$

where  $\phi$  is porosity,  $\phi_0$  is porosity on the surface,  $\phi_1$  is the irreducible porosity,  $b$  is a lithology-specific constant,  $z_e$  is the effective depth,  $\psi$  is fluid overpressure,  $\psi_{sc}$  is fluid overpressure on the surface,  $\rho_{sm}$  is the density of fluid saturated medium, and  $\rho$  is fluid density. The porosity is used to calculate the permeability using the following relationships:

$$\log k_x = A\phi + B \quad (11)$$

$$\frac{k_x}{k_z} = C \quad (12)$$

where  $k_x$  is the horizontal permeability,  $k_z$  is the vertical permeability, and  $A$ ,  $B$  and  $C$  are lithology-specific constants. The  $\phi$ ,  $k_x$  and  $k_z$  values obtained from these calculations are then used to solve Eq. (3) to obtain fluid overpressure ( $\psi$ ). Since porosity is dependent on the effective depth (Eq. (9)), which is in turn dependent on fluid overpressure (Eq. (10)), the sediment compaction equation (Eq. (2)) needs to be recalculated using the updated fluid overpressure values. The iteration between Eqs. (2) and (3) continues until the porosity values are converged. The numerical solution then proceeds to solve the heat conservation equation (Eq. (4)) to obtain the temperature values. When all the

governing equations (Eqs. (2)–(4)) are solved, a new time step starts. A new layer of nodal blocks is created at the top when a target thickness is reached after certain time steps. This procedure continues until sedimentation terminates. The numerical simulation thus reconstructs the evolution of the distribution of porosity, permeability, fluid overpressure, fluid flow velocity, temperature, and fraction of oil and gas generated throughout the history of the sedimentary basin.

## References

- Alexandre, P., Kyser, T.K., 2012. Modeling of the fluid flow involved in the formation of Athabasca basin unconformity-type uranium deposits. Geological Association of Canada–Mineralogical Association of Canada Annual Conference Abstracts, 35, p. 3.
- Alexandre, P., Kyser, K., Polito, P., Thomas, D., 2005. Alteration mineralogy and stable isotope geochemistry of Paleoproterozoic basement-hosted unconformity-type uranium deposits in the Athabasca Basin, Canada. *Econ. Geol.* 100, 1547–1563.
- Alexandre, P., Kyser, K., Polito, P., Marlat, J., 2009. Geochronology of unconformity-related uranium deposits in the Athabasca Basin, Saskatchewan, Canada and their integration in the evolution of the basin. *Miner. Deposita* 44, 41–59.
- Alt-Epping, P., Zhao, C., 2010. Reactive mass transport modeling of a three-dimensional vertical fault zone with a finger-like convective flow regime. *J. Geochem. Explor.* 106, 8–23.
- Annesley, I.R., Madore, C., Shi, R., Krogh, T.E., 1997. U–Pb geochronology of thermotectonic events in the Wollaston Lake area, Wollaston Domain: a summary of 1994–1996 results. In: Summary of Investigations 1997. Saskatchewan Geological Survey, Saskatchewan Energy and Mines, Miscellaneous Report, 97–4, pp. 162–173.
- Annesley, I.R., Madore, C., Cutler, J., 2001. Synchrotron X-ray analysis of graphitic pelitic gneisses in the vicinity of unconformity-type uranium mineralization. In: Summary of Investigations 2001. Saskatchewan Geological Survey, Saskatchewan Energy and Mines, Miscellaneous Report 2001–4.2, vol. 2, pp. 132–140.
- Appold, M.S., Garven, G., 2000. Reactive flow models of ore formation in the southeast Missouri district. *Econ. Geol.* 95, 1605–1626.
- Awadh, S.M., Ali, K.K., Alazzawi, A.T., 2013. Geochemical exploration using surveys of spring water, hydrocarbon and gas seepage, and geobotany for determining the surface extension of Abu-Jir Fault Zone in Iraq: a new way for determining geometrical shapes of computational simulation models. *J. Geochem. Explor.* 124, 218–229.
- Bethke, C.M., 1985. A numerical model of compaction-driven groundwater flow and heat transfer and its application to paleohydrology of intracratonic sedimentary basins. *J. Geophys. Res.* 90, 6817–6828.
- Bethke, C.M., Marshak, S., 1990. Brine migration across North America – the plate tectonics of groundwater. *Annu. Rev. Earth Planet. Sci.* 18, 287–315.
- Bethke, C.M., Lee, M.K., Quinodoz, H., Kreiling, W.N., 1993. Basin Modeling with Basin2, a Guide to Using Basin2, B2Plot, B2Video, and B2View. University of Illinois, Urbana (225 pp.).
- Boiron, M.-C., Cathelineau, M., Richard, A., 2010. Fluid flows and metal deposition near basement/cover Fluid flows and metal deposition near basement /cover unconformity: lessons and analogies from Pb–Zn–F–Ba systems for the understanding of Proterozoic U deposits. *Geofluids* 10, 270–292.
- Card, C.D., Pana, D., Portella, P., Thomas, D.J., Annesley, I.R., 2007. Basement rocks of the Athabasca basin, Saskatchewan and Alberta. In: Jefferson, C.W., Delaney, G. (Eds.), EXTECH IV: Geology and Uranium Exploration Technology of the Proterozoic Athabasca Basin, Saskatchewan and Alberta. Geological Survey of Canada Bulletin, 588, pp. 69–87.
- Cathles, L.M., 1981. Fluid flow and genesis of hydrothermal ore deposits. *Economic Geology* 75th Anniversary Volume. 424–457.
- Charifo, G., Almeida, J.A., Ferreira, A., 2013. Managing borehole samples of unequal lengths to construct a high-resolution mining model of mineral grades zoned by geological units. *J. Geochem. Explor.* 132, 209–223.
- Chi, G., 2001. BsnMod: a Windows program for simulating basin-scale fluid flow and heat transfer processes related to sediment compaction and tectonic uplifting in two dimensions. Geological Survey of Canada, Current Research 2001D–24. (7 pp.).
- Chi, G., Savard, M.M., 1998. Basinal fluid flow models related to Zn–Pb mineralization in the southern margin of the Maritimes Basin, eastern Canada. *Econ. Geol.* 93, 896–910.
- Chi, G., Xue, C., 2011. An overview of hydrodynamic studies of mineralization. *Geosci. Front.* 2, 423–438.
- Chi, G., Qing, H., Xue, C., Zeng, R., 2006. Modeling of fluid pressure evolution related to sediment loading and thrust faulting in the Lanping Basin – implications for the formation of the Jinding Zn–Pb deposit, Yunnan, China. *J. Geochem. Explor.* 89, 57–60.
- Chi, G., Lavoie, D., Bertrand, R., Lee, M.K., 2010. Downward hydrocarbon migration predicted from numerical modeling of fluid overpressure in the Paleozoic Anticosti Basin, eastern Canada. *Geofluids* 10, 334–350.
- Chi, G., Bosman, S., Card, C., 2011. Fluid flow models related to uranium mineralization in the Athabasca Basin: a review and new insights. Saskatchewan Geological Survey Open House 2011, Saskatoon, Abstract Volume. 4.
- Chi, G., Bosman, S., Card, C., 2013. Numerical modeling of fluid pressure regime in the Athabasca Basin and implications for fluid flow models related to the unconformity-type uranium mineralization. *J. Geochem. Explor.* 125, 8–19.
- Creaaser, R.A., Stasiuk, L.D., 2007. Depositional age of the Douglas Formation, northern Saskatchewan, determined by Re–Os geochronology. In: Jefferson, C.W., Delaney, G. (Eds.), EXTECH IV: Geology and Uranium Exploration Technology of the Proterozoic Athabasca Basin, Saskatchewan and Alberta. Geological Survey of Canada Bulletin, 588, pp. 341–346.
- Cui, T., Yang, J., Samson, I.M., 2012. Tectonic deformation and fluid flow: implications for the formation of unconformity-related uranium deposits. *Econ. Geol.* 107, 147–163.

- Cuney, M., Brouand, M., Cathelineau, M., Derome, D., Freiberger, R., Hecht, L., Kister, P., Lobaev, V., Lorilleux, G., Peiffert, C., Bastoul, A.M., 2003. What parameters control the high-grade-large tonnage of Proterozoic unconformity related uranium deposits? Proceedings of International Conference on Uranium Geochemistry, Nancy, France, pp. 123–126.
- Derome, D., Cathelineau, M., Cuney, M., Farbe, C., Lhomme, T., 2005. Mixing of sodic and calcic brines and uranium deposition at McArthur River, Saskatchewan, Canada: a Raman and laser-induced breakdown spectroscopic study of fluid inclusions. *Econ. Geol.* 100, 1529–1545.
- Garven, G., 1985. The role of regional fluid flow in the genesis of the Pine Point deposit, Western Canada sedimentary basin. *Econ. Geol.* 80, 307–324.
- Garven, G., 1989. A hydrogeologic model for the formation of the giant oil sands deposits of the Western Canada Sedimentary Basin. *Am. J. Sci.* 289, 105–166.
- Garven, G., 1995. Continental-scale groundwater flow and geologic processes. *Annu. Rev. Earth Planet. Sci.* 23, 89–117.
- Gow, P., Upton, P., Zhao, C., Hill, K., 2002. Copper–Gold mineralization in the New Guinea: numerical modeling of collision, fluid flow and intrusion-related hydrothermal systems. *Aust. J. Earth Sci.* 49, 753–771.
- Harrison, W.J., Summa, L.L., 1991. Paleohydrogeology of the Gulf of Mexico basin. *Am. J. Sci.* 291, 109–176.
- Hiatt, E., Kyser, K., 2007. Sequence stratigraphy, hydrostratigraphy, and mineralizing fluid flow in the Proterozoic Manitou Falls Formation, eastern Athabasca Basin, Saskatchewan. In: Jefferson, C.W., Delaney, G. (Eds.), EXTECH IV: Geology and uranium exploration technology of the Proterozoic Athabasca Basin, Saskatchewan and Alberta. Geological Survey of Canada Bulletin, 588, pp. 489–506.
- Hobbs, B.E., Zhang, Y., Ord, A., Zhao, C., 2000. Application of coupled deformation, fluid flow, thermal and chemical modelling to predictive mineral exploration. *J. Geochem. Explor.* 69, 505–509.
- Hoeve, J., Quirt, D.H., 1984. Uranium mineralization and host-rock alteration in relation to clay mineral diagenesis and evolution of the Middle Proterozoic Athabasca Basin, Northern Saskatchewan, Canada. Saskatchewan Research Council. Technical Report, 187 (187 pp.).
- Hoeve, J., Sibbald, T., 1978. On the genesis of Rabbit Lake and other unconformity-type uranium deposits in northern Saskatchewan, Canada. *Econ. Geol.* 73, 1450–1473.
- Hubbert, M.K., 1953. Entrapment of petroleum under hydrodynamic conditions. *AAPG Bull.* 37, 1954–2026.
- Ingebritsen, S.E., Appold, M.S., 2012. The physical hydrogeology of ore deposits. *Econ. Geol.* 107, 559–584.
- Jefferson, C.W., Thomas, D.J., Gandhi, S.S., Ramaekers, P., Delaney, G., Brisbane, D., Cutts, C., Portella, P., Olson, R.A., 2007. Unconformity-associated uranium deposits of the Athabasca Basin, Saskatchewan and Alberta. In: Jefferson, C.W., Delaney, G. (Eds.), EXTECH IV: Geology and Uranium Exploration Technology of the Proterozoic Athabasca Basin, Saskatchewan and Alberta. Geological Survey of Canada Bulletin, 588, pp. 23–67.
- Jones, J.C., 2010. Hydrocarbons – Physical Properties and their Relevance to Utilization. Jones & Ventus Publishing (111 pp.).
- Ju, M., Zhao, C., Dai, T., Yang, J., 2011. Finite element modeling of pore-fluid flow in the Dachang ore district, Guangxi, China: implications for hydrothermal mineralization. *Geosci. Front.* 2 (3), 463–474.
- Kaufman, J., 1994. Numerical models of fluid flow in carbonate platforms: implications for dolomitization. *J. Sediment. Res.* 64, 128–139.
- Khalil, A., Hanich, I., Bannari, A., Zouhri, I., Pourret, O., Hakkou, R., 2013. Assessment of soil contamination around an abandoned mine in a semi-arid environment using geochemistry and geostatistics: pre-work of geochemical process modeling with numerical models. *J. Geochem. Explor.* 125, 117–129.
- Kyser, T.K., Cuney, M., 2008. Unconformity-related uranium deposits. In: Cuney, M., Kyser, M. (Eds.), Recent and Not-So-Recent Developments in Uranium Deposits and Implications for Exploration. Mineralogical Association of Canada Short Course Series, 39, pp. 161–220.
- Kyser, T.K., Wilson, M.R., Ruhmann, G., 1989. Stable isotope constraints on the role of graphite in the genesis of unconformity-type uranium deposits. *Can. J. Earth Sci.* 26, 490–498.
- Kyser, T.K., Hiatt, E., Renac, C., Durocher, K., Holk, G., Deckart, K., 2000. Diagenetic fluids in paleo- and meso-Proterozoic sedimentary basins and their implications for long protracted fluid histories. In: Kyser, T.K. (Ed.), Fluid and Basin Evolution. Mineralogical Association of Canada Short Course, 28, pp. 225–262.
- Landis, P., Dubessy, J., Dereppe, J.-M., Philp, R.P., 1993. Characterization of graphite alteration and bitumen genesis in the Cigar Lake deposit (Saskatchewan, Canada). *Can. J. Earth Sci.* 30, 743–753.
- Lee, M.K., Williams, D.D., 2000. Paleohydrogeology of the Delaware Basin, western Texas: overpressure development, hydrocarbon migration, and ore genesis. *AAPG Bull.* 84, 961–974.
- Leventhal, J.S., Grauch, R.I., Threlkeld, C.N., Lichte, F.E., 1987. Unusual organic matter associated with uranium from the Claude deposit, Cluff Lake, Canada. *Econ. Geol.* 82, 1169–1176.
- Lin, G., Zhao, C., Hobbs, B.E., Ord, A., Muhlhaus, H.B., 2003. Theoretical and numerical analyses of convective instability in porous media with temperature-dependent viscosity. *Commun. Numer. Methods Eng.* 19, 787–799.
- Lin, G., Zhou, Y., Wei, X., Zhao, C., 2006. Structural controls on pore-fluid flow and related mineralization in the Xiangshan Uranium deposit, Southern China. *J. Geochem. Explor.* 89, 231–234.
- Lin, G., Zhao, C., Hobbs, B.E., Zhang, L., Zhou, Y., 2008. Potential effects of upward throughflow on thermal structure models within the continental lithospheric mantle-crust. *Chin. J. Geophys.* 51 (2), 393–401.
- Lin, G., Peng, M., Zhao, C., Zhang, L., Zhang, D., Liu, S., 2009. Numerical analysis and simulation experiment of lithospheric thermal structures in the South China Sea and the Western Pacific. *J. Earth Sci.* 20, 85–94.
- Liu, L., Yang, G., Peng, S., Zhao, C., 2005. Numerical modelling of coupled geodynamical processes and its role in facilitating predictive ore discovery: an example from Tongling, China. *Resour. Geol.* 55, 21–31.
- Liu, L., Shu, Z., Zhao, C., Wan, C., Cai, A., Zhao, Y., 2008. The controlling mechanism of ore formation due to flow-focusing dilation spaces in skarn ore deposits and its significance for deep-ore exploration: examples from the Tongling-Anqing district. *Acta Petrol. Sin.* 24, 1848–1856.
- Liu, L., Zhao, Y., Zhao, C., 2010. Coupled geodynamics in the formation of Cu skarn deposits in the Tongling-Anqing district, China: computational modeling and implications for exploration. *J. Geochem. Explor.* 106, 146–155.
- Liu, L., Wan, C., Zhao, C., Zhao, Y., 2011. Geodynamic constraints on orebody localization in the Anqing orefield, China: computational modeling and facilitating predictive exploration of deep deposits. *Ore Geol. Rev.* 43, 249–263.
- McCready, A.J., Annesley, I.R., Parnell, J., Richardson, L.C., 1999. Uranium-bearing carbonaceous matter, McArthur River uranium deposit, Saskatchewan. In: Summary of Investigations 1999. Saskatchewan Geological Survey, Saskatchewan Energy and Mines, Miscellaneous Report 99-4.2, vol. 2, pp. 110–120.
- Mercadier, J., Richard, A., Cathelineau, M., 2012. Boron- and magnesium-rich marine brines at the origin of giant unconformity-related uranium deposits:  $\delta^{11}\text{B}$  evidence from Mg-tourmalines. *Geology* 40, 231–234.
- Mugler, C., Rabouille, C., Bombled, B., Montarnal, P., 2012. Impact of spatial heterogeneities on oxygen consumption in sediments: experimental observations and 2D numerical modeling. *J. Geochem. Explor.* 112, 76–83.
- Norton, D., 1978. Source lines, source regions, and pathways for fluids in hydrothermal systems related to cooling plutons. *Econ. Geol.* 73, 21–28.
- Oliver, N.H.S., McLellen, J.G., Hobbs, B.E., Cleverley, J.S., Ord, A., Feltrin, L., 2006. Numerical models of extensional deformation, heat transfer and fluid flow across basement-cover interfaces during basin-related mineralization. *Econ. Geol.* 101, 1–31.
- Ord, A., Hobbs, B.E., Zhang, Y., Broadbent, G.C., Brown, M., Willetts, G., Sorjonen-Ward, P., Walshe, J., Zhao, C., 2002. Geodynamic modeling of the Century deposit, Mt. Isa Province, Queensland. *Aust. J. Earth Sci.* 49, 1011–1039.
- Orrell, S.E., Bickford, M.E., Lewry, J.F., 1999. Crustal evolution and age of thermotectonic reworking in the western hinterland of Trans-Hudson orogen, northern Saskatchewan. *Precambrian Res.* 95, 187–223.
- Page, M., 1975. Détermination des conditions physico-chimiques de la silicification diagenétique des grès Athabasca (Canada) au moyen des inclusions fluides. *C. R. Acad. Sci. Paris* 280, 2301–2304.
- Pepper, A.S., Corvi, P.J., 1995. Simple kinetic models of petroleum formation. Part I: oil and gas generation from kerogen. *Mar. Pet. Geol.* 12, 291–319.
- Pepper, A.S., Dodd, T.A., 1995. Simple kinetic models of petroleum formation. Part II: oil-gas cracking. *Mar. Pet. Geol.* 12, 321–340.
- Peters, K.E., Walters, C.C., Mankiewicz, P.J., 2006. Evaluation of kinetic uncertainties in numerical models of petroleum generation. *AAPG Bull.* 90, 387–403.
- Raffensperger, J.P., Garven, G., 1995. The formation of unconformity type uranium ore deposits: 1. Coupled groundwater flow and heat transport modeling. *Am. J. Sci.* 295, 581–636.
- Rainbird, R.H., Stern, R.A., Rayner, N., Jefferson, C.W., 2007. Age, provenance, and regional correlation of the Athabasca Group, Saskatchewan and Alberta, constrained by igneous and detrital zircon geochronology. In: Jefferson, C.W., Delaney, G. (Eds.), EXTECH IV: Geology and Uranium Exploration Technology of the Proterozoic Athabasca Basin, Saskatchewan and Alberta. Geological Survey of Canada Bulletin, 588, pp. 193–209.
- Ramaekers, P., Jefferson, C.W., Yeo, G.M., Collier, B., Long, D.G.F., Drever, G., McHardy, S., Jiricka, D., Cutts, C., Wheatley, K., Catuneanu, O., Bernier, S., Kupsch, B., Post, R.T., 2007. Revised geological map and stratigraphy of the Athabasca Group, Saskatchewan and Alberta. In: Jefferson, C.W., Delaney, G. (Eds.), EXTECH IV: Geology and Uranium Exploration Technology of the Proterozoic Athabasca Basin, Saskatchewan and Alberta. Geological Survey of Canada Bulletin, 588, pp. 155–191.
- Richard, A., Banks, D.A., Mercadier, J., Boiron, M.-C., Cuney, M., Cathelineau, M., 2011. An evaporated seawater origin for the ore-forming brines in unconformity-related uranium deposits (Athabasca Basin, Canada): Cl/Br and  $\delta^{37}\text{Cl}$  analyses of fluid inclusions. *Geochim. Cosmochim. Acta* 75, 2792–2810.
- Schaubs, P., Zhao, C., 2002. Numerical modelling of gold-deposit formation in the Bendigo-Ballarat zone, Victoria. *Aust. J. Earth Sci.* 49, 1077–1096.
- Schmidt, Mumm, A., Brugger, J., Zhao, C., Schacht, U., 2010. Fluids in geological processes: the present state and future outlook. *J. Geochem. Explor.* 106, 1–7.
- Scott, R., Chi, G., Bosman, S., 2011. A petrographic and fluid inclusion study of the Athabasca Group sandstones from the Rumpel Lake drill core, Athabasca Basin, Northern Saskatchewan. In: Summary of Investigations 2011. Saskatchewan Geological Survey, Saskatchewan Energy and Resources, Miscellaneous Report 2011-4.2, Paper A5, vol. 2 (10 pp.).
- Sorjonen-Ward, P., Zhang, Y., Zhao, C., 2002. Numerical modeling of orogenic processes and mineralization in the south eastern part of the Yilgarn Craton, Western Australia. *Aust. J. Earth Sci.* 49, 935–964.
- Speight, J.G., 2006. The Chemistry and Technology of Petroleum, 4th edition. CRC Press, Taylor & Francis Group (984 pp.).
- Stasiuk, L.D., Fowler, M.G., Jiricka, D., Mossison, D., Sopuck, V., Wheatley, K., Wilson, N.S., Zaluski, G., 2001. Preliminary investigation into organic petrology and Athabasca Group sandstones distal and proximal to uranium mineralization, Athabasca basin, Saskatchewan. In: Summary of Investigations 2001. Saskatchewan Geological Survey, Saskatchewan Energy and Mines, Miscellaneous Report 2001-4.2, vol. 2, pp. 224–239.
- Sung, K.Y., Yun, S.T., Park, M.E., Koh, Y.K., Choi, B.Y., Hutcheon, I., Kim, K.H., 2012. Reaction path modeling of hydrogeochemical evolution of groundwater in granitic bedrocks, South Korea. *J. Geochem. Explor.* 118, 90–97.

- Swarbrick, R.E., Osborne, M.J., Yardley, G.S., 2002. Comparison of overpressure magnitude resulting from the main generating mechanisms. In: Huffman, A.R., Bowers, G.L. (Eds.), *Pressure Regimes in Sedimentary Basins and their Prediction*. AAPG Memoir, 76, pp. 1–12.
- Wilson, N.S.F., Stasiuk, S.L., Fowler, M.G., 2007. Origin of organic matter in the Proterozoic Athabasca Basin of Saskatchewan and Alberta, and significance to unconformity uranium deposits. In: Jefferson, C.W., Delaney, G. (Eds.), *EXTECH IV: Geology and Uranium Exploration Technology of the Proterozoic Athabasca Basin, Saskatchewan and Alberta*. Geological Survey of Canada Bulletin, 588, pp. 325–339.
- Xing, H.L., Makinouchi, A., Zhao, C., 2008. Three-dimensional finite element simulation of large-scale nonlinear contact friction problems in deformable rocks. *J. Geophys. Eng.* 5, 27–36.
- Xue, C., Chi, G., Xue, W., 2010. Interaction of two fluid systems in the formation of sandstone-hosted uranium deposits in the Ordos Basin: geochemical evidence and hydrodynamic modeling. *J. Geochem. Explor.* 106, 226–235.
- Xue, C., Chi, G., Xue, W., 2011. Effects of hydrocarbon generation on fluid flow in the Ordos Basin and relationship with uranium mineralization. *Geosci. Front.* 2, 439–447.
- Zhang, Y., Hobbs, B.E., Ord, A., Barnicoat, A., Zhao, C., Lin, G., 2003. The influence of faulting on host-rock permeability, fluid flow and ore genesis of gold deposits: a theoretical 2D numerical model. *J. Geochem. Explor.* 78–79, 279–284.
- Zhang, Y., Schaub, P.M., Zhao, C., Ord, A., Hobbs, B.E., Barnicoat, A., 2008. Fault-related dilation, permeability enhancement, fluid flow and mineral precipitation patterns: numerical models. In: Wibberley, C.A.J., Kurz, W., Imber, J., Holdsworth, R.E., Collettini, C. (Eds.), *The Internal Structure of Fault Zones: Implications for Mechanical and Fluid-flow Properties*. Geological Society, vol. 299, Special Publications, London, pp. 239–255.
- Zhang, L., Li, Z., Zhao, C., Lin, G., Guo, H., 2011a. Numerical simulation of effects of upward throughflow on thermal structure and the thickness of the continental lithosphere. *J. Geophys. Eng.* 8, 322–329.
- Zhang, Y., Robinson, J., Schaub, P.M., 2011b. Numerical modeling of structural controls on fluid flow and mineralization. *Geosci. Front.* 2, 449–461.
- Zhao, C., Mühlhaus, H.B., Hobbs, B.E., 1997. Finite element analysis of steady-state natural convection problems in fluid-saturated porous media heated from below. *Int. J. Numer. Anal. Methods Geomech.* 21, 863–881.
- Zhao, C., Hobbs, B.E., Baxter, K., Mühlhaus, H.B., Ord, A., 1999. A numerical study of pore-fluid, thermal and mass flow in fluid-saturated porous rock basins. *Eng. Comput.* 16, 202–214.
- Zhao, C., Hobbs, B.E., Ord, A., Peng, S., Mühlhaus, H.B., Liu, L., 2004. Theoretical investigation of convective instability in inclined and fluid-saturated three-dimensional fault zones. *Tectonophysics* 387, 47–64.
- Zhao, C., Hobbs, B.E., Ord, A., Hornby, P., Peng, S., Liu, L., 2007. Mineral precipitation associated with vertical fault zones: the interaction of solute advection, diffusion and chemical kinetics. *Geofluids* 7, 3–18.
- Zhao, C., Hobbs, B.E., Ord, A., 2008a. *Convective and Advective Heat Transfer in Geological Systems*. Springer, Berlin.
- Zhao, C., Hobbs, B.E., Ord, A., 2008b. Investigating dynamic mechanisms of geological phenomena using methodology of computational geosciences: an example of equal-distant mineralization in a fault. *Sci. China Ser. D Earth Sci.* 51, 947–954.
- Zhao, C., Hobbs, B.E., Ord, A., Hornby, P., Peng, S., 2008c. Morphological evolution of three-dimensional chemical dissolution front in fluid-saturated porous media: a numerical simulation approach. *Geofluids* 8, 113–127.
- Zhao, C., Hobbs, B.E., Ord, A., Hornby, P., Peng, S., 2008d. Effect of reactive surface areas associated with different particle shapes on chemical-dissolution front instability in fluid-saturated porous rocks. *Transp. Porous Media* 73, 75–94.
- Zhao, C., Hobbs, B.E., Ord, A., 2009. *Fundamentals of Computational Geoscience: Numerical Methods and Algorithms*. Springer, Berlin.
- Zhao, C., Hobbs, B.E., Ord, A., 2010. Theoretical analyses of nonaqueous-phase-liquid dissolution induced instability in two-dimensional fluid-saturated porous media. *Int. J. Numer. Anal. Methods Geomech.* 34, 1767–1796.
- Zhao, C., Hobbs, B.E., Regenauer-Lieb, K., Ord, A., 2011. Computational simulation for the morphological evolution of nonaqueous-phase-liquid dissolution fronts in two-dimensional fluid-saturated porous media. *Comput. Geosci.* 15, 167–183.
- Zhao, C., Reid, L.B., Regenauer-Lieb, K., 2012a. Some fundamental issues in computational hydrodynamics of mineralization: a review. *J. Geochem. Explor.* 112, 21–34.
- Zhao, C., Hobbs, B.E., Ord, A., 2012b. Effects of domain shapes on the morphological evolution of nonaqueous-phase-liquid dissolution fronts in fluid-saturated porous media. *J. Contam. Hydrol.* 138–139, 123–140.